

Environmental force sensing enables robots to traverse cluttered obstacles with interaction

Qihan Xuan, Yaqing Wang, Chen Li¹

Abstract—Many applications require robots to move through terrain with large obstacles, such as self-driving, search and rescue, and extraterrestrial exploration. Although robots are already excellent at avoiding sparse obstacles, they still struggle in traversing cluttered obstacles. Inspired by cockroaches that use and respond to physical interaction with obstacles in various ways to traverse grass-like beams with different stiffness, here we developed a physics model of a minimalistic robot capable of environmental force sensing propelled forward to traverse two beams to simulate and understand the traversal of cluttered obstacles. Beam properties like stiffness and deflection locations could be estimated from the noisy beam contact forces measured, whose fidelity increased with sensing time. Using these estimates, the model predicted the cost of traversal defined using potential energy barriers and used it to plan and control the robot to generate and track a trajectory to traverse with minimal cost. When encountering stiff beams, the simulation robot transitioned from a more costly pitch mode to a less costly roll mode to traverse. When encountering flimsy beams, it chose to push cross beams with less energy cost than avoiding beams. Finally, we developed a physical robot and demonstrated the usefulness of the estimation method.

Index Terms—locomotion, terradynamics, physical property

I. INTRODUCTION

Mobile robots are becoming increasingly important in society. Many important tasks require robots to move through complex terrain with large obstacles (comparable to robot size or larger), such as furniture in household chores [1], buildings, vehicles, and pedestrians in self-driving [2], rubble in search and rescue [3], and rocks in extraterrestrial exploration [4]. A common strategy to move in such environments is to avoid obstacles [5], [6]. To do so, imaging sensors such as cameras build a geometric map of the environment, and a collision-free trajectory is devised to help the robot move around obstacles [7], [8]. Such a geometry-based obstacle avoidance approach works well in environments where obstacles are sparse [1], [2].

However, obstacle avoidance is often challenged in environments with cluttered obstacles. First, a collision-free path may not exist. Second, a collision-free path may be energetically too expensive or require a very long time to execute, because the robot needs to take a long detour to avoid obstacles. Furthermore, if not avoiding obstacles in time, unexpected collisions and contact could cause robots to flip over and damage [9], [10].

By contrast, animals constantly have physical interaction with obstacles on complex terrain (e.g. cockroach [11], lizard [12], snake [13], [14]). In some cases, obstacles even benefit the locomotion, such as snakes undulate forward by pushing

obstacles (e.g., grass, rocks, sticks) [13]–[15]. To study the locomotor-obstacle interaction in cluttered terrain [16], our lab studies that cockroaches’ traversal on complex 3D terrain cluttered with diverse types of large obstacles like bumps, gaps, pillars, and grass-like beams [11], [17]–[19] (for a review, see [20]). We observed that they can even maintain a high speed and stability during traversal while having many physical interactions with obstacles. We studied the animal-obstacle interaction and designed bioinspired robots to move through complex terrain using physical interaction with obstacles [11], [18], [19], [21]. By exploiting body-obstacle interaction, robots modified its body shape [11], [19] and added feedforward control [17], [21] to improve their locomotor performance, such as traversing a large bump with a pitched-up, head-on body orientation [18], traversing beam gaps narrower than the robot’s width by body oscillations [21], and traversing terrain with multi pillars with a rounded body shape [19].

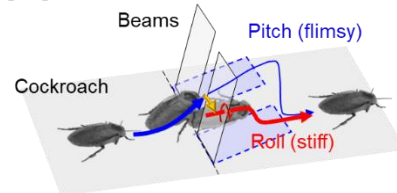


Fig. 1. Cockroach beam traversal experiments show how cockroach traverses different beams.

Further understanding cockroaches’ performance will further advance bioinspired robots. Cockroaches have feedback control and can actively adjust their body and appendages [22] to perform better than open-loop robots (e.g., using less body oscillations to traverse beams by head, abdomen, and leg adjustment [21], [22], climbing higher bumps by body and leg adjustment [18]). In addition, active adjustment is sensitive to the physical properties of obstacles [22]. For example, cockroaches simply push down flimsy beams while pitching up the body to traverse, whereas they often transition from pitching to rolling into a gap and maneuvering through. This is because pushing across flimsy beams overcomes a low potential energy barrier, but for stiff beams doing so requires overcoming a larger potential energy barrier than rolling through gaps [21] (Fig. 1, blue is the pitch mode, red is the roll mode, and orange is transition from the pitch to roll mode). Cockroaches cannot differentiate stiff and flimsy beams before contact. Thus, it is likely that they sense how stiff the obstacles are during contact and then choose the less costly locomotor mode to traverse. This inspired us that environmental force sensing may help robots to do active adjustment when traversing cluttered obstacles.

Environmental force sensing has been used widely in robotics to measure contact forces when contacting with

¹Department of Mechanical Engineering, Johns Hopkins University.
Corresponding author: chen.li@jhu.edu, <https://li.me.jhu.edu>

targets/environment. Forces data can be further used to calculate the relative positions and poses, deformation, and physical properties of contacted objects. For example, force sensing helps mobile robots to obtain surface properties of ground [23], [24], detect the instant of contact and separation with obstacles/ground [25], and correct localization errors [26], to better exploit the robot-environment interaction. However, few of them studied how it helps robots estimate the physical properties of cluttered obstacles to choose an appropriate locomotor mode to traverse.

Inspired by the locomotor transitions in cockroach beam traversal and applications of forcing sensing to infer environmental physics, here we develop a physics model to demonstrate how environmental force sensing can help a robot actively adjust its body to better traverse cluttered obstacles with the body-obstacle interaction than using feedforward control only. Our previous study developed a potential energy landscape approach to understand the emergence of locomotor modes and transitions from locomotor-terrain interaction [21], but it did not consider dynamics. Here, we added a contact force model, equations of motion, and force/torque controllers and performed dynamic simulations.

The cockroach-inspired robot was modelled as an ellipsoidal body and propelled forward to encounter grass-like beams (Sec. II, A). We first simulated beam traversal without active control. With sufficient propulsion, the simulation robot pushed down and traversed flimsy beams. However, when beams were stiff, the robot was stuck in front of beams. Simply increasing propulsion may cause flipping over (Sec. III, A).

Then, we used the environmental force sensing to estimate the stiffness of beams and added active control to the simulation robot (Sec. II, C-I). The theoretical contact force with beams was used to generate the sensing data. Gaussian noise was added into it to simulate the effect of collisional dynamics and sensing errors. Simulation results showed that the estimated stiffness and deflection locations of beams were close to true values under a certain noise level (Sec. III, Bii). In addition, we found that the more unknown parameters in the physics model, the lower the accuracy of the estimation and the worse the robustness to noise (Sec. III, Biii). Using these estimates, the model built the potential energy landscape, which helped to plan a trajectory with the minimal energy barrier (Sec. II, H). The model also predicted the current external forces and states to help in feedback control (Sec. II, I). With control, the robot pushed down flimsy beams, whereas the robot rolled through the gap of beams when encountering stiff beams (Sec. III, C), whose behaviors were similar to what cockroaches did. When the robot traversed flimsy beams, we found the energy cost decreased compared with the obstacle avoidance strategy (Sec. III, D).

For robots and animals, sensing, signal processing, motion planning, and motor delay take time (referred to as "sensory delay" below, defined in Sec. II, E) before reacting to the collision. In simulation, we found the varying sensory delay changed the initial state in motion planning, which influenced the energy cost in traversal (Sec. III, E).

Considering that the model was simplified in contact

mechanics and beam dynamics which could lead to large errors in estimating beam properties, we built a well-controlled robot with a force sensor to test how well our estimation method works in a physical system (Sec. IV). The robot experiments showed that the estimation of unknown parameters was closed to the true values. Finally, we discuss the limitations of our method and its broader applications and future work (Sec. V).

II. METHODS

A. *Physics model of traversing beams*

The simulation robot followed the minimalistic design in our previous study [21]. It was modelled as a rigid ellipsoid similar to the discoid cockroach's body [21], with principal axes lengths $2a = 0.24$ m, $2b = 0.14$ m, and $2c = 0.06$ m, and mass $M = 0.2$ kg (Fig. 2A). The center of the rotation overlaps with the geometric center. The center of mass is lower than the center of rotation by $h_c = 0.02$ m (Fig. 2A), so that the robot is stable at zero roll and zero pitch (Euler angles: yaw γ , pitch β , and roll α , Z - Y' - X' Tait-Bryan convention). The moments of inertia along the three principal axes are $(I_1, I_2, I_3) = (2, 5, 7) \times 10^{-3}$ kg·m². The geometric center is $H = 0.06$ m from the ground. For simplicity, it is constrained to only move along the forward x direction and rotate in roll and pitch directions. Thus, the robot has three degrees of freedom. An external forward force F_x is added at the geometric center to model the propulsion from legs, and two external torques τ_1 and τ_2 are added to model the effect of active leg adjustment during traversal. F_x , τ_1 , and τ_2 are set to zero before the robot contacts the beams to simulate a stable gait of the cockroach/robot with a constant speed $v_x = 0.05$ m/s (0.21 body length per second) before collision. After collision, if there is no active control, F_x is set to be a constant, and τ_1 and τ_2 are still zero because there is no active leg adjustment.

For simplicity, the grass-like beams are modelled as rigid, vertical plates with torsion springs. Each beam has two unknown parameters, the stiffness k of the spring and the height of the deflection point h_b (Fig. 2B). The beam deflects at one point as a simplification of a cantilever beam (e.g., grass) that can bend throughout its length. Compared to the beam position, the beam deflection point is more challenging to detect and measure. Thus, h_b is set to an unknown parameter whereas beam positions are known. The grass is usually much lighter than the robot, thus, beams are approximated to be massless. Massless beams will not bounce away but keep contact with the robot when pushed down.

The two beams are at $x = 0$ m, aligning with the y axis, and vertical to the ground when there is no deflection (Fig. 2B). The gap width between two beams is $d = 0.12$ m, which is narrower than the width of the robot (Fig. 2A). The center line of the gap is the x axis. The width and height of each beam are $w = 0.05$ m and $L = 0.16$ m. The center of the robot is always on the center line of the beam gap.

Because a smooth shell is a good design for robots to reduce resistance, we assumed that the surface of the simulation robot is smooth, resulting in no frictional force at contact with beams. Thus, the contact force between the robot and each beam is normal to the tangent plane of the contact point on the

ellipsoid (Fig. 2C). In addition, because the beams are massless, the collisional forces are negligible.

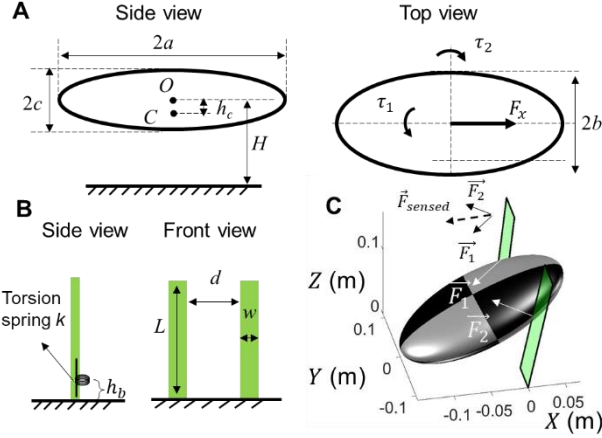


Fig. 2. Physics model of robot-beam interaction. (A) Cockroach-inspired robot is modeled as an ellipsoid rigid body. F_x is the propulsive force. τ_1 and τ_2 are external roll and pitch torques. (B) Each beam is modeled as a rigid plate with a torsion spring. Stiffness is k . Deflection point is h_b above ground. (C) \vec{F}_1 and \vec{F}_2 are contact forces with each beam. \vec{F}_{sensed} is the sum of the contact forces measured by environmental force sensing.

B. Dynamics: Equations of motion of simulation robot

Besides the input force F_x and torques (τ_1 , τ_2) from controllers acting on the simulation robot, there are three external forces, which are the gravitational force \vec{G} and contact forces (\vec{F}_1 , \vec{F}_2) with two beams (Fig. 2C). According to Newton's second law and Euler's rotation equations, the equations of motion of the robot are:

$$I\dot{\omega}_1 = \tau_1 + (\vec{r}_{11} \times \vec{F}_1 + \vec{r}_{12} \times \vec{F}_2 + \vec{r}_{1M} \times \vec{G}) \cdot \vec{e}_1 \quad (1)$$

$$I\dot{\omega}_2 = \tau_2 + (\vec{r}_{21} \times \vec{F}_1 + \vec{r}_{22} \times \vec{F}_2 + \vec{r}_{2M} \times \vec{G}) \cdot \vec{e}_2 \quad (2)$$

$$M\dot{v}_x = F_x + \vec{F}_1(1) + \vec{F}_2(1) \quad (3)$$

where \vec{r}_{ij} ($i, j = 1, 2$) is the shortest displacement from the i^{th} principal axis to the point of application of \vec{F}_j , ω_i is the angular velocity along the i^{th} principal axis. \vec{e}_1 and \vec{e}_2 are the unit vector along the major and intermediate principal axes.

The time step in all simulation is 0.0002 s, making the numerical error in position smaller than 0.1 mm in all trials.

C. Contact force model

Because beams are massless, each beam maintains torque equilibrium during contact.

$$k_i \theta_i + \vec{r}_{bi} \times \vec{F}_i \cdot (0, 1, 0) = 0 \quad (4)$$

where k_i is the stiffness of the i^{th} beam, θ_i is its beam deflection angle, \vec{r}_{bi} is the shortest displacement from the rotational axis of the i^{th} beam to the point of application of \vec{F}_i .

The normal direction to an ellipsoid at (x, y, z) is:

$$\vec{n} = (b^2 c^2 x, a^2 c^2 y, a^2 b^2 z) \quad (5)$$

Thus, each beam contact force acting at (x, y, z) is along \vec{n} in the body frame. Given current orientation of the simulation robot and Eqns. 4 and 6, we can calculate contact forces \vec{F}_1 and \vec{F}_2 in the world frame.

D. Simulating environmental force sensing

Contact forces were calculated based on the torque

equilibrium (Sec. II, C). In the simulation, we assumed that a force sensor measured total contact forces ($\vec{F} = \vec{F}_1 + \vec{F}_2$) with a sampling rate of 100 Hz (Fig. 2C). However, in real situations, beams have mass and inertia, which leads to collisions and intermittent contact [27]. Thus, real forces should vary around values of torques calculated from the torque equilibrium. In addition, sensors have measurement errors. To simulate these effects, Gaussian noise $Z \sim \mathcal{N}(0, \sigma)$ is added into contact forces $\vec{F}_{sensed}(t)$.

$$\vec{F}_{sensed} = \vec{F}(1 + Z) \quad (6)$$

We assumed that the noise is proportional to \vec{F} because the deviation from the actual value may increase as the contact becomes more intense. The standard deviation σ varies from 5%, 10%, 20%, and 50% (Fig. 3).

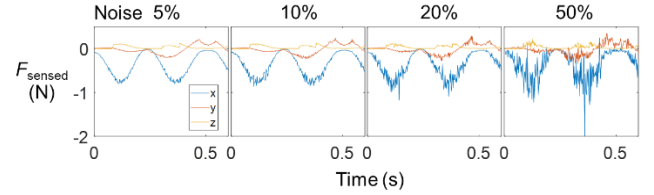


Fig. 3. Contact forces measured by sensor with different levels of noise. Data shown is from a trial of stiff beams traversal.

E. Solving unknown beam properties

Forces measured by the force sensor during sensing time $T_s = 300$ ms, which is the time interval after the instant of first contact, are used to calculate unknown parameters k and h_b of each beam. We fitted the theoretical contact force \vec{F} to the force data \vec{F}_{sensed} by minimizing the error between the two (using the MATLAB `fminsearch` function):

$$e = \sum_{i=1}^N |\vec{F}_{sensed}(t_i) - \vec{F}(k_1, k_2, h_{b1}, h_{b2}, t_i)| \quad (7)$$

where N is the total number of the sampling force data points. This process was repeated 100 times with different initial guess of parameter values randomly selected, increasing the likelihood of finding a global minimum. Specifically, initial values of $k_{1,2}$ and $h_{b1,2}$ are selected from uniformly distributed random numbers in the range $[0, 5]$ N·m/rad and $[0, 5]$ mm, respectively.

F. Potential energy landscape

There are two different locomotor modes to traverse stiff and flimsy beams, which are the pitch and roll modes [21]. To determine a less costly mode, we calculated the potential energy barrier during the entire traversal. Potential energy of the system consists of gravitational potential energy of the robot and the elastic potential energy of beams:

$$E(x, \alpha, \beta) = MgZ_{CoM}(\alpha, \beta) + \frac{1}{2}k_1\theta_1(x, \alpha, \beta)^2 + \frac{1}{2}k_2\theta_2(x, \alpha, \beta)^2. \quad (8)$$

where $Z_{CoM}(\alpha, \beta)$ is the height of center of mass.

We varied x from -0.12 m to 0.12 m with an increment $\Delta x = 0.002$ m and α and β from -90° to 90° with an increment $\Delta\alpha (\Delta\beta) = 2^\circ$ to obtain a 3-D potential energy landscape over the entire (α, β, x) workspace during traversal (Fig. 4A).

G. Less costly locomotor mode

Using the potential energy landscape, we calculated the

critical stiffness that differentiates flimsy and stiff beams, for which the pitch and roll modes overcome a lower potential energy barrier, respectively. For simplicity, we assumed that deflection locations of the beams were known ($h_{b1} = h_{b2} = 0$), and two beams had the same stiffness ($k_1 = k_2 = k_0$) to estimate the potential energy barrier using each mode (this simplification only applies to this section). For the roll mode, the potential energy reaches the maximum when the robot rolls until no contact in the entire traversal. Thus, its potential energy barrier is $PE_{roll} \sim Mgh_c$. For the pitch mode, the potential energy reaches the maximum when the robot is on beams. Thus, its potential energy barrier is $PE_{pitch} \sim k \cdot \arccos(H, L)^2$. Because PE_{roll} does not depend on beam stiffness whereas PE_{pitch} is proportional to it, the barrier difference $PE_{pitch} - PE_{roll}$ monotonically increases with k . Above $k_0 = \frac{Mg h_c}{\arccos(H, L)^2}$, the roll mode overcomes a lower barrier, and below it the pitch mode overcomes a lower barrier. Thus, we defined beams with stiffness above k_0 as stiff beams, and those with stiffness below k_0 as flimsy beams.

H. Motion planning

To further obtain the quantitative planned trajectory in x , roll, and pitch space, a cost of each trajectory is defined to measure the difficulty of traversal. A directed graph is created based on the energy landscape built in Sec. II, F. We defined the states in the energy landscape as vertices and the connections between vertices as directed edges. Each vertex connects with its six closest neighbors, which are $(x \pm \Delta x, \alpha, \beta)$, $(x, \alpha \pm \Delta \alpha, \beta)$, and $(x, \alpha, \beta \pm \Delta \beta)$ (Fig. 4B). A path in the network is composed of vertices and directed edges. Thus, the total cost of a path is the sum of the cost of all directed edges within it. The cost of a directed edge is defined by its direction and potential energy difference between the two states it connects. For the robot to move to a state with higher potential energy along a directed edge, the actuator needs do work. Thus, the cost of this directed edge is positive and defined as this potential energy increases. For the robot to move to a state with a lower potential energy along a directed edge, the decrease in potential energy can transform into kinetic energy. In this case, we assumed that the actuators do no work and the cost of the directed edge is zero (Fig. 4B).

For each trajectory, we defined the initial state as the state after the sensory delay and the target state to be the state with the horizontal pose ($\alpha = \beta = 0$) after traversal. Sensory delay Δt is defined as the time interval from the instant of first contact with beams t_c to the instance when active control began t_s , i.e., $\Delta t = t_s - t_c$. Dijkstra's algorithm [28] is used to search for the minimal cost path between the initial and target states in the directed graph (Fig. 4C). The planned path is a series of discrete state data \vec{q}_d connected with directed edges. To apply feedback control, a trajectory, which is a state function of time, is needed. We first added a timeline into the path to obtain $\vec{q}_d[t]$, with a time interval of 0.02 s between two vertices. Then, we used three fifth order polynomials $f_x(t)$, $f_\alpha(t)$, and $f_\beta(t)$ to fit $\vec{q}_d[t]$ using the MATLAB function "polyfit". Finally, we obtained the state function about time $\vec{q}_d(t) = [f_x(t); f_\alpha(t); f_\beta(t)]$.

I. Motion control

After motion planning, we controlled the simulation robot to track the planned trajectory. Given dynamic equations of the robot (Eqns. 1-3), we used feedback linearization control [29] to obtain the control input at every 0.002 s:

$$\vec{u} = \mathbf{M}\ddot{\vec{q}}_d - K_d(\dot{\vec{q}} - \dot{\vec{q}}_d) - K_p(\vec{q} - \vec{q}_d) + F(\vec{q}) \quad (9)$$

where $\vec{q} = (x, \alpha, \beta)$ is the current state, and $\vec{q}_d = (x_d, \alpha_d, \beta_d)$ is the desired state. K_d and K_p are positive feedback gains. $\mathbf{M} = [I_1, 0, 0; 0, I_2, 0; 0, 0, M]$ is the inertia matrix. $\vec{u} = (\tau_1, \tau_2, F_x)$ is the control input. $F(\vec{q})$ is the external force including contact forces with beams and the gravitational force. $\dot{\vec{q}}_d(t)$ and $\ddot{\vec{q}}_d(t)$ are the first and second time derivatives of $\vec{q}_d(t)$, respectively. The physics model (Eqns. 1-4) can predict the current external forces $F(\vec{q})$ and states \vec{q} . With the control input \vec{u} , the current state is controlled to approach to the desired state at every time step.

To avoid extremely large forces/torques input that may exceed actuator capacity, we set limits for them ($|F_x| \leq 2$ N, $|\tau_1| \leq 0.1$ N·m, $|\tau_2| \leq 0.1$ N·m) so that acceleration $|a_x| \leq 10$ m·s⁻², angular acceleration $|\beta_1| \leq 50$ rad·s⁻², $|\beta_2| \leq 20$ rad·s⁻². When \vec{u} calculated from Eqn. 9 exceed limits, \vec{u} is set to be the maximum or minimum values within limit.

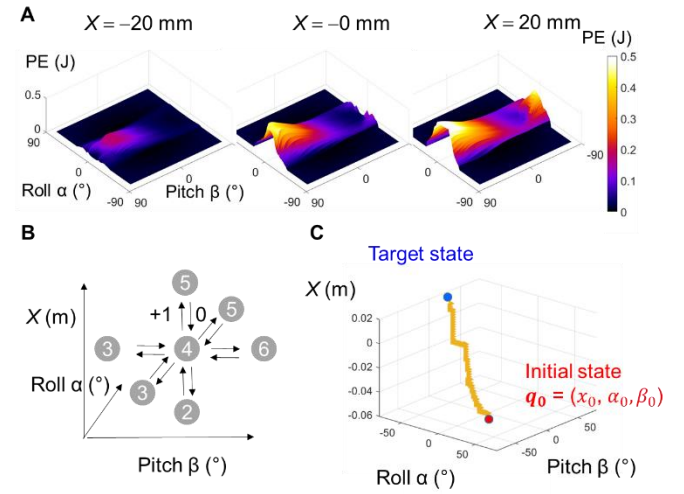


Fig. 4. Motion planning. (A) 3-D potential energy landscape. (B) Schematic of the directed graph based on potential energy landscape. Circles are states. Values in circles show representative potential energy at each state. (C) Minimal cost path.

III. SIMULATION RESULTS

A. Traversing flimsy and stiff beams without control

We first simulated the robot traversing flimsy and stiff beams without force feedback control ($F_x = 0.1$ or 1 N, $\tau_1 = \tau_2 = 0$ N·m).

Substituting the values of parameters given in the model design (Sec. II, A), the critical value of stiffness was $k_0 = 0.028$ N·m/rad. Thus, we chose $k_{low} = 0.01$ N·m/rad and $k_{high} = 0.25$ N·m/rad as stiffness of flimsy and stiff beams, respectively.

For a small propulsive force $F_x = 0.1$ N, the robot could not push down neither flimsy or stiff beams and got stuck in front (Fig. 5A; Multimedia Material). For a larger $F_x = 1$ N, the

robot could traverse the flimsy beams by pushing them down and moving over them (Fig. 5B, bottom; Multimedia Material). However, for the stiff beams, increasing to $F_x = 1$ N caused the robot to flip over (Fig. 5B, top; Multimedia Material). Thus, for the open-loop robot, even a strong propulsion may not help the robot escape from being trapped in the pitch mode, and it was more likely to flip over by simply increasing propulsion especially when encountering stiff obstacles.

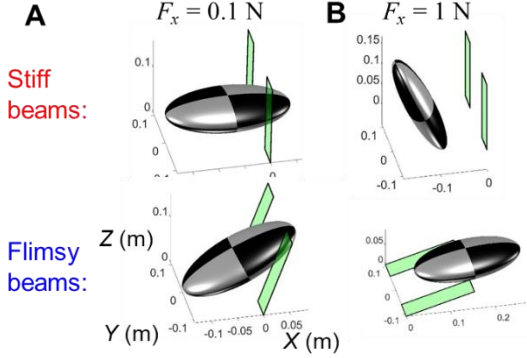


Fig. 5. Typical snapshots of simulation without control to traverse stiff and flimsy beams with $F_x = 0.1$ N (A) and 1 N (B).

B. Estimating beam properties in simulation

i. Estimation of parameters without noise in sensing

The robot was propelled by $F_x = 1$ N to encounter beams. True values of stiffness of beams were $k_1 = 0.25$ and $k_2 = 0.27$ N·m/rad, and deflection locations were $h_{b1} = h_{b2} = 0$ mm.

Using the sensed force data, we obtained the estimated values of unknown parameters were $h_{b1} = h_{b2} = 0$ mm and $k_1 = 0.25$, $k_2 = 0.27$ N·m/rad, which were the same as the true values. It showed that the search algorithm found the global minimum with a limited number of initial guesses without noise.

ii. Estimation of parameters with different levels of noise in force data

The noise in force data increased the difficulty to estimate the unknown parameters. Following the similar steps in the previous section, unknown parameters of beams were estimated from force data with different levels of noise and the relative error of each estimated value was calculated (Table 1). For k_1 and k_2 , the relative error was the ratio of the estimated error and its true value, $e_{ki} = \frac{|k_i - k_i|}{k_i}$. For h_{b1} and h_{b2} , the relative error was the ratio of estimated error and the range ($\Delta h = 5$ mm) of the initial guess, $e_{hi} = \frac{|h_{bi} - h_{bi}|}{\Delta h}$. As noise increased, estimation accuracy generally decreased (Table 1-3). In addition, the estimation accuracy of deflection locations was more sensitive to the noise level than the estimation of the stiffness. When the noise level was larger than 10%, the estimation relative error of the deflection location was larger than 100%. But among the noise levels we tested, the estimation of stiffness was close to the true values (relative error < 30%).

Table 1. Estimation of 4 unknown parameters with noise. Unit of k_i is N·m/rad, h_{bi} is mm.

Noise	5%	10%	20%	50%
-------	----	-----	-----	-----

$\widehat{k}_1(e_{k1})$	0.264(5%)	0.273(9%)	0.253(1%)	0.274(10%)
$\widehat{k}_2(e_{k2})$	0.283(5%)	0.355(30%)	0.306(13%)	0.344(27%)
$\widehat{h}_{b1}(e_{h1})$	1.57(31%)	3.33(67%)	1.40(28%)	1.82(36%)
$\widehat{h}_{b2}(e_{h1})$	1.39(28%)	9.77(195%)	5.14(102%)	6.84(137%)

iii. Estimation with fewer unknown parameters

Furthermore, to study the effect of the number of unknown parameters on estimation accuracy and robustness to noise, we tested the cases with two and three unknown parameters in beam properties and compared them with results of four unknown parameters. In the case with three unknown parameters, we assumed that deflection locations of two beams were the same ($h_{b1} = h_{b2}$). In the case with two unknown parameters, we assumed that deflection locations of beams were known ($h_{b1} = h_{b2} = 0$ mm). Estimation results and relative errors are shown in Table 2 and 3, respectively.

Table 2. Estimation of 3 unknown parameters with noise

Noise	5%	10%	20%	50%
$\widehat{k}_1(e_{k1})$	0.257(3%)	0.243(3%)	0.239(5%)	0.336(34%)
$\widehat{k}_2(e_{k2})$	0.278(3%)	0.263(3%)	0.259(4%)	0.258(33%)
$\widehat{h}_b(e_{h1})$	0.92(18%)	1.37(27%)	0.58(12%)	7.34(147%)

With four unknown parameters, relative errors of k_1 and k_2 were both around 5% when noise was 5%. With three unknown parameters, to have the same accuracy level, its noise was allowed to be 20%. With two unknown parameters, the accuracy was 5% even when the noise was 50%. Comparison among the three cases showed that the fewer unknown parameters, the better the estimation. This revealed that the more information in advance to have and the fewer unknown parameters, the more robust estimation was to the noise in force data.

Table 3. Estimation of 2 unknown parameters with noise

Noise	5%	10%	20%	50%
$\widehat{k}_1(e_{k1})$	0.250(0%)	0.252(1%)	0.244(2%)	0.262(5%)
$\widehat{k}_2(e_{k2})$	0.270(0%)	0.273(1%)	0.265(2%)	0.284(5%)

iv. The effect of the sensing time in estimation

We studied how estimation accuracy depends on sensing time. We tested sensing time $T_s = 50, 100, 300$, and 600 ms. A longer sensing time means more data points can be used in model fitting. As expected, an increase in sensing time improved estimation accuracy as sensing time increased from 50 to 300 ms (Table 4). However, for sufficiently large numbers of the data points (sensing time ≥ 300 ms), improvement in estimation accuracy diminished (Table 4).

Table 4. Estimation of 3 unknown parameters with noise $\sigma = 20\%$ for different sensing time

T_s	50 ms	100 ms	300 ms	600 ms
$\widehat{k}_1(e_{k1})$	0.090(24%)	0.229(8%)	0.239(5%)	0.270(8%)
$\widehat{k}_2(e_{k2})$	0.100(63%)	0.248(8%)	0.259(4%)	0.290(7%)
$\widehat{h}_b(e_{h1})$	22(440%)	1.92(38%)	0.58(12%)	0.79(16%)

C. Traversing beams with interaction and control

Using the estimated values of parameters of beams in Sec.

III, B (three unknown parameters, k_1 , k_2 , h_b ; noise $\sigma = 20\%$), we constructed a potential energy landscape and performed motion planning (Sec. II, F-H).

For flimsy beams ($k_{low} = 0.01$ N·m/rad), the planned trajectory was pitching up and moving over beams. For stiff beams ($k_{high} = 0.25$ N·m/rad), the planned trajectory was rolling through the gap. Then, we controlled the robot to track planned trajectories to traverse two kinds of beams. The simulation results showed that the control method worked well and the traversal was successful in both cases (Fig. 6; Multimedia Material).

These results showed that the motion planning and control using the sensed environmental force information generated the same traversal strategies to traverse beams when encountering the flimsy and stiff beams as observed in cockroaches (Fig. 1).

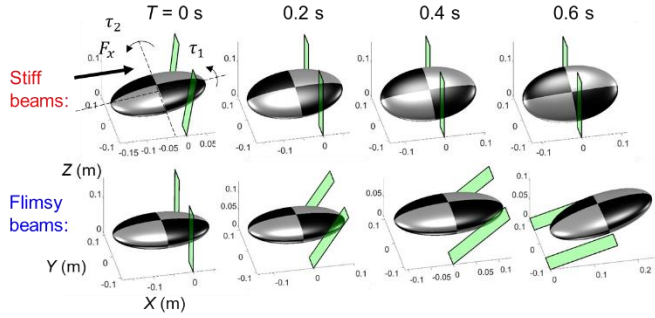


Fig. 6. Robot traversed stiff and flimsy beams under motion control.

D. Traversing beam by avoiding obstacles

We also used the obstacle-avoidance strategy to control the robot to traverse beams. Based on the geometric map, the robot rolled its body to traverse beams, regardless of beams were stiff or flimsy (Multimedia Material).

We compared the traversal performance of the obstacle-avoidance strategy with the strategy using physical interaction. For stiff beams, two strategies had similar traversal behaviors. For flimsy beams, two strategies had different behaviors.

To compare the energy cost of different strategies, we defined the energy cost as the work done by actuators in the entire traversal:

$$E_{cost} = \sum_{i=1}^m [(F_x v_x)^+ + (\tau_1 \omega_1)^+ + (\tau_2 \omega_2)^+] dt \quad (11)$$

where m was the number of control input in the entire traversal time, $dt = 0.002$ s was the control time step (Sec. II, I). $(F_x v_x)^+$ was the power of the force F_x . $(\tau_1 \omega_1)^+$ and $(\tau_2 \omega_2)^+$ were the powers of two torques (τ_1, τ_2) . The symbol “+” meant $(f)^+ = \max\{f, 0\}$. We added it because we assumed that actuators would not restore energy.

For stiff beams, $E_{cost} = 52$ mJ using the obstacle-avoidance strategy, and $E_{cost} = 60$ mJ using the interaction with obstacles strategy. The interaction with obstacles strategy costed 15% more energy because the robot deflected the beams in the beginning. The obstacle avoidance strategy costs energy to just keep the body rolled up, whereas the animal and robot can actually lean against the beams between the gap. In addition, the animal can grasp and pull/push against the beams to assist traversal. We did not model these effects in simulation and likely overestimated its cost. If we take these

into account, traversal using physical interaction will likely cost less than the obstacle avoidance strategy.

For flimsy beams, $E_{cost} = 52$ mJ using the obstacle-avoidance strategy, and $E_{cost} = 21$ mJ using the interaction with obstacles strategy. The interaction strategy saved 60% energy because the pitch mode overcame a lower energy barrier than the roll mode.

E. Traversal performance with different sensory delay

Here, we used our simulation to study the influence of sensory delay on the traversal performance. We tested three different sensory delay, 100, 300, and 600 ms in simulation. We calculated the energy cost from actuators (Eqn. 11) for trials of different sensory delay.

The longer the sensory delay was, the more the robot pitched up when it started active control (Fig. 7A). Despite this, the robot successfully traversed in all trials (Multimedia Material). We found that the longer the sensory delay, the more energy cost from actuators (Fig. 7B). This means that the faster the robot could estimate obstacle properties and respond after encountering obstacles, the more energy it would save.

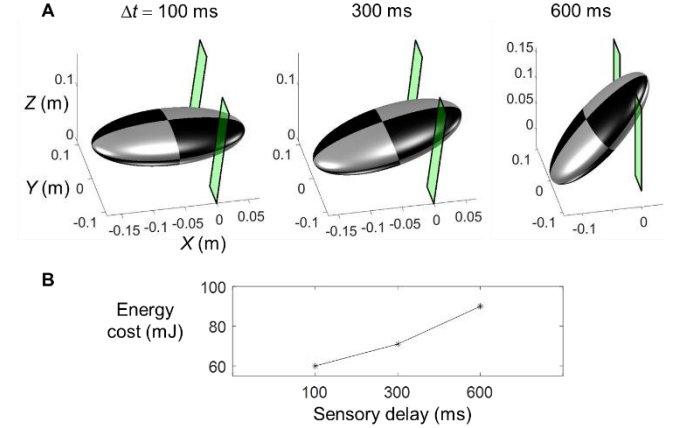


Fig. 7. Influence of sensory delay. (A) States after different sensory delay. (B) Energy cost with different sensory delay.

IV. ROBOTIC EXPERIMENTAL VALIDATION

A robotic physical model (Fig. 8) was built based on the design of the physics model (Fig. 2) to demonstrate the usefulness of our modeling approach for estimating unknown beam parameters. A robot moved towards two beams, with a force sensor measuring contact forces.

An ellipsoidal robot ($a = 0.19$ m, $b = 0.09$ m, $c = 0.035$ m; 0.8 kg, center of mass was 3 mm below geometric center) was made using 3-D printing. The robot was suspended under a level rail via a gyroscope mechanism (similar to that in [21]) to allow passive pitch and roll rotations with little friction, but no yaw rotation. We installed two beams (height $L = 0.305$ m, width $w = 0.1$ m, mass $M_B = 0.16$ kg, thickness $\delta = 6$ mm for each beam) made of acrylic, with gap width $d = 0.15$ m. The middle of the gap was aligned with the rail. The robot was allowed to translate only along fore-aft direction (Fig. 8B). A servo motor and a rack and pinion mechanism were used to precisely control the translational forward and speed of the robot. The center of rotation overlapped with the geometric

center of the robot. Using a force sensor with a sampling rate of 100 Hz (ATI Mini40) on the support rod that drove the robot forward (Fig. 8B), we measured the change in the force compared to the static state, which was sum of the total contact force with the beams and the inertial force of the robot. To capture the robot's position and orientation, we used four synchronized high-speed cameras to record robot and beam motions at 200 frame/s and a resolution of 1920×1080 pixels from side, oblique top, isometric, and rear views (Fig. 8B).

Beam stiffness used in robot experiments were $k_1 = k_2 = 0.78 \text{ N}\cdot\text{m}/\text{rad}$. There were preloaded torques to keep beam vertical, which were $\tau_{01} = \tau_{02} = 0.19 \text{ N}\cdot\text{m}$ but unknown a priori. In the model, we assumed that the two beams had the same properties and deflection location was known, so there were only two unknown parameters, k and τ_0 . Considering that beam mass $M_B = 0.16 \text{ kg}$ was not negligible in experiments, we included it, as well as the preloaded torque, in the torque equilibrium equation:

$$\tau_{0i} + k_i \theta_i + \vec{r}_{bi} \times \vec{F}_i \cdot (0, 1, 0) - \frac{L}{2} M_B g = 0 \quad (12)$$

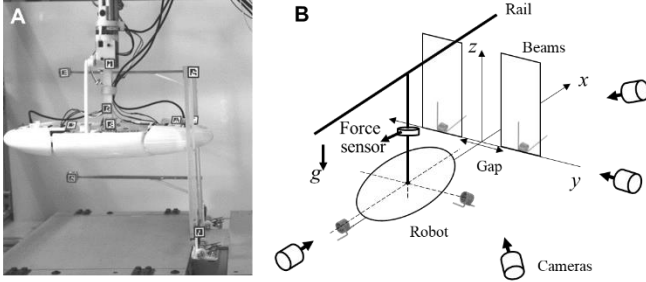


Fig. 8. Robotic physical model. (A) Sideview photo of robotic physical model. (B) Isometric schematic of experimental setup.

Before each trial, we set the robot to be far away from the beams with no contact, with an equilibrium horizontal pose ($\alpha, \beta = 0$), and set the beams vertical. The robot was then driven forward at a constant speed of 0.064 m/s . As it came in contact with the beams, the robot pitched up due to contact forces and pushed the beams down. We performed three trials. Using BEEtags [30] for automatic tracking and direct linear transformation for 3-D reconstruction [31], we measured the positions and orientations of the robot as a function of time, interpolated them to 100 Hz, and synchronized them with force and torque data.

Using force data collected during traversal in robot experiments, the average estimated value of stiffness was $\hat{k} = 0.67 \text{ N}\cdot\text{m}/\text{rad}$, whose relative error was 14%. The estimated value of the preloaded torque was $\hat{\tau}_0 = 0.21 \text{ N}\cdot\text{m}$, whose relative error was 11%. These results demonstrated the usefulness of the estimation method.

V. DISCUSSION

We developed a beam traversal physics model with the force/torque controllers, the contact force model, and robot dynamics. This dynamic model allowed us to simulate the robot motion quantitatively when encountering beam obstacles. Our simulation demonstrated that environmental force sensing can help estimate the beam properties which were unknown a priori. The estimated beam parameters

helped choose a less costly locomotor mode and trajectory with the minimal cost in motion planning. The estimation method is robust to noise in force data and was useful in a physical robot. In addition, our simulation results showed that this predictive model helped in control to better traverse beams. We plan to validate it by robot experiments in future.

We discuss limitations of our work and future directions. In this paper, we modeled obstacles as rigid plates with torsion springs. However, obstacle models can be various. We can have different designs to model different obstacles. For example, the beam weight and preloaded torques were added into the beam model in our robot experiments. By updating unknown parameters, the fitting method still worked. In addition, the effects of friction and damping can be added in the model. Considering different types of deformation, we can also have the cantilever model that can deflect at any point, the elastic rod model that can deflect in all directions, the movable rigid body model (e.g., rock, box), etc. Not only unknown parameters in obstacles, but also uncertain states of robots, such as the position and orientation, can be estimated from contact forces. In general, if the contact force can be expressed by a function of parameters of obstacles and the robot state, we can sense the contact forces to estimate them.

The more complex obstacle model usually has more unknown parameters, which poses a challenge to the accuracy of estimation. The estimation ability can be improved by adding more sensors. For example, in our model, the single force sensor can only measure the sum of contact forces from different contact points. If there are more sensors measuring contact forces with each beam, it can be predicted that the accuracy in estimation will improve.

The predictive, physics model not only helps in estimating unknown parameters, but also helps in control. The feedback control (Eqn. 9) requires the robot state and the external forces in real time. However, because there is time delay in sensors, the actual control input is calculated using the state and external forces in the previous moment. When velocities and/or accelerations are large, the control may not be timely and may lead to unexpected collisions. In this case, the physics model can predict the state and external forces, which can help better control timely.

In the motion planning, the planned trajectory was based on the potential energy landscape but did not consider the inertia of the robot. In addition, the way we added the timeline into a series of sequential states may not be optimal in cost and time. To improve it, an optimal control based on our physics model can be applied. The cost function can be set as the total energy cost (Eqn. 12). The optimal trajectory is the one that minimizes the cost function. But there are some problems, such as the contact force is not a smooth function of the state and the global minimum is difficult to find. We are exploring applying optimal control method.

In addition to robotics, our work also informs biological sensing and locomotion on complex terrain. Cockroaches transitioning from the pitch to roll mode after collisions with stiff beams suggests that, besides using vision [32] and

antennae to sense the environment geometrically [33], animals likely sense obstacle physical properties (e.g., using load-sensitive receptors in insects [34]) when traversing cluttered obstacles. Studying this will be fruitful as has been the case in geometry sensing [32] or tactile sensing of environment with sparse obstacles [33].

ACKNOWLEDGMENTS

We thank Ratan Othayoth for discussion. This work was supported by an Arnold & Mabel Beckman Foundation Beckman Young Investigator Award, a Burroughs Wellcome Fund Career Award at the Scientific Interface, and The Johns Hopkins University Whiting School of Engineering start-up funds to C.L. Author contributions: Q.X. and C.L. conceived study; Q.X. designed study, developed the physics model, performed simulation, and analyzed data; Y.W. constructed the robot and did robot experiments; and Q.X. and C.L. wrote the paper with input from Y.W.

REFERENCES

- [1] B. Tribelhorn and Z. Dodds, "Evaluating the roomba: A low-cost, ubiquitous platform for robotics research and education," *Proc. - IEEE Int. Conf. Robot. Autom.*, pp. 1393–1399, 2007.
- [2] S. Thrun, W. Burgard, and D. Fox, "Real-time algorithm for mobile robot mapping with applications to multi-robot and 3D mapping," *Proc. - IEEE Int. Conf. Robot. Autom.*, vol. 1, no. April, pp. 321–328, 2000.
- [3] A. H. Reddy, B. Kalyan, and C. S. N. Murthy, "Mine Rescue Robot System – A Review," *Procedia Earth Planet. Sci.*, vol. 11, pp. 457–462, 2015.
- [4] M. Bostock, S. Carter, J. Corum, and W. Jeremy, "28 months on Mars," *The New York Times*, 2014.
- [5] E. Rimon and D. E. Koditschek, "Exact robot navigation using artificial potential functions," *IEEE Trans. Robot. Autom.*, vol. 8, no. 5, pp. 501–518, 1992.
- [6] J. Borenstein and Y. Koren, "The vector field histogram-fast obstacle avoidance for mobile robots - Robotics and Automation, IEEE Transactions on," *IEEE Trans. Robot.*, vol. 7, no. 3, pp. 278–288, 1991.
- [7] A. Elfes, "Using occupancy grids for mobile robot perception and navigation," *Computer (Long. Beach. Calif.)*, vol. 22, pp. 46–57, 1989.
- [8] M. W. M. Gamini Dissanayake, P. Newman, S. Clark, H. F. Durrant-Whyte, and M. Csorba, "A solution to the simultaneous localization and map building (SLAM) problem," *IEEE Trans. Robot. Autom.*, vol. 17, no. 3, pp. 229–241, 2001.
- [9] E. Guizzo and E. Ackerman, "The hard lessons of DARPA's robotics challenge [News]," *IEEE Spectr.*, vol. 52, no. 8, pp. 11–13, 2015.
- [10] C. Li, C. C. Kessens, R. S. Fearing, and R. J. Full, "Mechanical principles of dynamic terrestrial self-righting using wings," *Adv. Robot.*, vol. 31, no. 17, pp. 881–900, 2017.
- [11] C. Li, A. O. Pullin, D. W. Haldane, H. K. Lam, R. S. Fearing, and R. J. Full, "Terradynamically streamlined shapes in animals and robots enhance traversability through densely cluttered terrain," *Bioinspiration and Biomimetics*, vol. 10, no. 4, 2015.
- [12] S. E. Parker and L. D. McBrayer, "The effects of multiple obstacles on the locomotor behavior and performance of a terrestrial lizard," *J. Exp. Biol.*, vol. 219, no. 7, pp. 1004–1013, 2016.
- [13] B. C. Jayne, "Kinematics of Terrestrial Snake Locomotion," *Copeia*, pp. 915–927, 1986.
- [14] H. C. Astley, "Long limbless locomotors over land: The mechanics and biology of elongate, limbless vertebrate locomotion," *Integr. Comp. Biol.*, vol. 60, no. 1, pp. 134–139, 2020.
- [15] D. J. Jurestovsky, L. U. Usher, and H. C. Astley, "Generation of Propulsive Force via Vertical Undulations in Snakes," *J. Exp. Biol.*, 2021.
- [16] F. Qian and D. E. Koditschek, "An obstacle disturbance selection framework: emergent robot steady states under repeated collisions," *Int. J. Rob. Res.*, vol. 39, no. 13, pp. 1549–1566, 2020.
- [17] S. W. Gatt, C. Yan, R. Othayoth, Z. Ren, and C. Li, "Dynamic traversal of large gaps by insects and legged robots reveals a template," *Bioinspiration and Biomimetics*, vol. 13, no. 2, p. 026006, 2018.
- [18] S. W. Gatt and C. Li, "Body-terrain interaction affects large bump traversal of insects and legged robots," *Bioinspiration and Biomimetics*, vol. 13, no. 2, p. 026005, 2018.
- [19] Y. Han *et al.*, "Shape-induced obstacle attraction and repulsion during dynamic locomotion," *Int. J. Rob. Res.*, vol. 40, no. 6–7, pp. 939–955, 2021.
- [20] R. Othayoth, Q. Xuan, Y. Wang, and C. Li, "Locomotor transitions in the potential energy landscape-dominated regime," *Proceedings of the Royal Society B: Biological Sciences*, vol. 288, no. 1949, 2021.
- [21] R. Othayoth, G. Thoms, and C. Li, "An energy landscape approach to locomotor transitions in complex 3D terrain," *Proc. Natl. Acad. Sci. U. S. A.*, vol. 117, no. 26, pp. 14987–14995, 2020.
- [22] Y. Wang, R. S. Othayoth Mullankandy, and C. Li, "Active adjustments help cockroaches traverse obstacles by lowering potential energy barrier," in *Bulletin of the American Physical Society* 65, 2020.
- [23] S. Bhattacharya, A. Luo, S. Dutta, M. Miura-Mattausch, and H. J. Mattausch, "Force-sensor-based surface recognition with surface-property-dependent walking-speed adjustment of humanoid robot," *IEEE Access*, vol. 8, pp. 169640–169651, 2020.
- [24] R. D. Howe and M. R. Cutkosky, "Dynamic tactile sensing: perception of fine surface features with stress rate sensing," *IEEE Trans. Robot. Autom.*, vol. 9, no. 2, pp. 140–151, Apr. 1993.
- [25] B. Andrews, B. Miller, J. Schmitt, and J. E. Clark, "Running over unknown rough terrain with a one-legged planar robot," *Bioinspiration and Biomimetics*, vol. 6, no. 2, 2011.
- [26] D. Belter, P. Łabecki, and P. Skrzypczyński, "Adaptive Motion Planning for Autonomous Rough Terrain Traversal with a Walking Robot," *J. F. Robot.*, vol. 33, no. 3, pp. 337–370, May 2016.
- [27] M. Bühler, D. E. Koditschek, and P. J. Kindlmann, "A Family of Robot Control Strategies for Intermittent Dynamical Environments," *IEEE Control Syst. Mag.*, vol. 10, no. 2, pp. 16–22, 1990.
- [28] D. B. Johnson, "A Note on Dijkstra's Shortest Path Algorithm," *J. ACM*, vol. 20, no. 3, pp. 385–388, 1973.
- [29] J. Chiasson, "Dynamic Feedback Linearization of the Induction Motor," *IEEE Trans. Automat. Contr.*, vol. 38, no. 10, pp. 1588–1594, 1993.
- [30] J. D. Crall, N. Gravish, A. M. Mountcastle, and S. A. Combes, "BEEtag: A low-cost, image-based tracking system for the study of animal behavior and locomotion," *PLoS One*, vol. 10, no. 9, pp. 1–13, 2015.
- [31] T. L. Hedrick, "Software techniques for two- and three-dimensional kinematic measurements of biological and biomimetic systems," *Bioinspir. Biomim.*, vol. 3, no. 3, p. 034001, 2008.
- [32] C. M. Harley, B. A. English, and R. E. Ritzmann, "Characterization of obstacle negotiation behaviors in the cockroach, *Blaberus discoidalis*," *J. Exp. Biol.*, vol. 212, no. 10, pp. 1463–1476, 2009.
- [33] J. Okada and Y. Toh, "Active tactile sensing for localization of objects by the cockroach antenna," *J. Comp. Physiol. A Neuroethol. Sensory, Neural, Behav. Physiol.*, vol. 192, no. 7, pp. 715–726, 2006.
- [34] A. Ayali, E. Couzin-Fuchs, I. David, O. Gal, P. Holmes, and D. Knebel, "Sensory feedback in cockroach locomotion: current knowledge and open questions," *J. Comp. Physiol. A Neuroethol. Sensory, Neural, Behav. Physiol.*, vol. 201, no. 9, pp. 841–850, 2015.